



HAL
open science

Prediction of the vertebral strength using a finite element model derived from low-dose biplanar imaging: benefits of subject-specific material properties

Emilie Sapin - de Brosse, Erwan Jolivet, Christophe Travert, David Mitton,
Wafa Skalli

► To cite this version:

Emilie Sapin - de Brosse, Erwan Jolivet, Christophe Travert, David Mitton, Wafa Skalli. Prediction of the vertebral strength using a finite element model derived from low-dose biplanar imaging: benefits of subject-specific material properties. Spine, 2012. hal-02121730

HAL Id: hal-02121730

<https://hal.science/hal-02121730>

Submitted on 26 Jul 2022

HAL is a multi-disciplinary open access archive for the deposit and dissemination of scientific research documents, whether they are published or not. The documents may come from teaching and research institutions in France or abroad, or from public or private research centers.

L'archive ouverte pluridisciplinaire **HAL**, est destinée au dépôt et à la diffusion de documents scientifiques de niveau recherche, publiés ou non, émanant des établissements d'enseignement et de recherche français ou étrangers, des laboratoires publics ou privés.

Prediction of the Vertebral Strength Using a Finite Element Model Derived From Low-Dose Biplanar Imaging

Benefits of Subject-Specific Material Properties

Emilie Sapin-de Brosse , PhD , Erwan Jolivet , PhD , Christophe Travert , PhD , David Mitton , PhD , and Wafa Skalli , PhD

From the Arts et Metiers ParisTech, Bd de l'Hôpital, Paris, France.

Acknowledgment date: June 22, 2010. First revision date: March 7, 2011.

Second revision date: June 10, 2011. Acceptance date: June 11, 2011.

The manuscript submitted does not contain information about medical device(s)/drug(s).

No funds were received in support of this work. No benefits in any form have been or will be received from a commercial party related directly or indirectly to the subject of this manuscript.

Abstract:

Study Design. A finite element analysis on osteoporotic vertebrae.

Objective. This study aims to validate subject-specific finite element models (FEMs) derived from a low-dose imaging system (EOS, Biospace Med, France) for the prediction of vertebral strength. The vertebrae are submitted to an eccentric compression force leading to compression and anterior bending. Summary of **Background Data.** Given the aging population, osteoporosis and vertebral fractures are a major public health issue. A low bone mineral density (BMD) does not always explain incident fractures, and multifactorial analyses are required. In this context, FEMs based on quantitative computed tomography (QCT) have been proposed to predict vertebral strength *in vitro* or quantify effects of treatments. However, the clinical use of such a model for the *in vivo* follow-up of the whole spine is limited by the high-radiation dose induced by QCT and the lying position, which does not allow postural assessment with the same modality.

Methods. Fourteen vertebrae were modelled using a parametric meshing method. The mesh was subject-specific using geometric parameters computed on the 3-dimensional (3D) reconstructions obtained from the EOS biplanar radiographs. The contribution of cortical bone was taken into account by modeling a cortico cancellous shell whose properties were derived from experimental data. The effect of subject-specific bone Young's moduli derived from EOS vertebral areal BMD was quantified. The 3D position of the point-of-load application and the 3D orientation of the force was faithfully reproduced in the model to compare the predicted strength and experimental strength under the same loading conditions.

Results. The relative error of prediction decreased from 43% to 16% (2.5 times) when subject-specific mechanical properties, derived from EOS areal BMD, were implemented in the FEM compared with averaged material properties. The resulting subject-specific FEMs predicted vertebral strength with a level of significance close to the QCT-based models ($r^2_{\text{adjusted}} = 0.79$, root mean square error = 367 N).

Conclusion. This work underlines the potential of low-dose biplanar x-ray devices to make subject-specific FEMs for prediction of vertebral strength.

Key words: biomechanics , EOS , finite element , low-dose imaging , osteoporosis , subject-specific , vertebra .

Introduction

Osteoporosis is “a skeletal disorder characterized by compromised bone strength predisposing to an increased risk of fracture.”¹ Although bone mineral density (BMD) assessment is the gold standard method for osteoporosis diagnosis, a low BMD only explains 18% to 78% of vertebral strength,^{2–5} and two-thirds of the vertebral fractures escape clinical diagnosis.⁶ Hence, structural analyses with finite element models (FEM) were proposed to predict *in vitro* vertebral strength under controlled compression.^{7–9} To date, these models are based on quantitative computed tomography (QCT) measurements: the 3-dimensional (3D) geometry of the mesh and the local Young's moduli of each element are respectively deduced from the outlines and the densities assessed on the QCT slices. These models predict *ex vivo* strength of vertebral bodies in axial compression ($r^2 = 0.80–0.94$),^{7–10} but they are much less effective in the case of anterior bending ($r^2 = 0.34–0.79$).^{11, 12} Eccentric compression is known to be responsible for many vertebral fractures.^{13–15} Moreover, the use of QCT for the *in vivo* follow-up of the whole spine is limited by the susceptibility of the trunk to high-radiation doses, and by the lying position, which does not enable postural assessment to define the *in vivo* loading conditions. For these reasons, non irradiant or low-dose imaging is being actively researched. The EOS system (EOS Imaging, Paris, France) simultaneously takes biplanar head-to-feet radiographs, in standing position, with a dose more than 100 times lower than QCT for the 3D reconstruction.¹⁶ Fast and accurate 3D reconstructions of the spine are available from the EOS radiographs.^{17, 18} Furthermore, *in vitro* areal BMDs assessed with a dual-energy modality exhibited the same global error as the clinical “gold standard” dual x-ray absorptiometry.¹⁹ This areal BMD was correlated with vertebral cancellous

bone elasticity so that density–Young’s modulus relationships were proposed for subject-specific finite element modelling. ²⁰ Finally, descriptions of the 3D position of the gravity line relative to the centre of each thoracic or lumbar vertebra were made for asymptomatic and pathologic populations with different ages with the EOS system. ^{15, 21, 22} On the basis of these works, *in vivo* first evaluation of the loading conditions applied on the thoracolumbar spine may be possible. The aim of the study is to validate a subject-specific FEM, derived from the EOS biplanar radiographs, for the prediction of *in vitro* vertebral strength. The contribution of the subject specific bone mechanical properties is especially quantified. To induce anterior wedge fractures, the vertebrae are submitted to an eccentric compression force leading to compression and anterior bending. ²³

MATERIALS AND METHODS

Specimens

Fourteen fresh frozen vertebrae, from T11 to L2, were harvested from 5 cadavers (4 women, 1 man, 88 ± 14 years old). To have well-defined boundary conditions and to avoid disc modelling (which could not be subject-specific in this study), the vertebral discs were removed. Posterior elements were kept intact. No clinical history was available on the donors. Vertebrae with radiographic evidence of fracture were excluded.

EOS Scanning

The vertebrae were placed into the EOS cabin to have the caudocranial axis parallel to the vertical direction. A dual-energy scanning was performed on each vertebra (low energy: 70-kV peak, 250 mA; high energy: 120-kV peak, 250 mA, pixel size of 0.250 mm) to assess the anteroposterior areal BMD (aBMD in g/cm^2). This measurement was previously validated by comparing EOS accuracy and reproducibility with the dual x-ray absorptiometry densitometers’ characteristics. ¹⁹ The low-energy biplanar radiographs were also used to generate the 3D reconstruction of the vertebra. ^{17, 18}

Finite Element Modeling

Subject-Specific Mesh

Hexahedral parametric meshes were created using common volumes, ^{24, 25} whose shape and dimensions were controlled by 23 geometric parameters ([see Appendix, Supplemental Digital Content 1](#)). Two different parametric models were designed to match the specific shape of either the thoracic or the lumbar vertebral body. Fourteen independent geometric parameters (height, width, and depth of the vertebral body) were fully automatically computed from the 3D reconstructions ¹⁷ (see Appendix Figure 1, [Supplemental Digital Content 2](#); see Appendix Figure 2, [Supplemental Digital Content 3](#); see Appendix Figure 3, [Supplemental Digital Content 4](#)). The 4 parameters that described the geometry and the location of the pedicles were deduced from the previous ones using anatomical relationships. ^{17, 26} The global dimensions of the posterior arch were also automatically computed from the 3D reconstructions. ¹⁷ A generic mesh of this region, with these subject-specific global dimensions, was added to the mesh of the vertebral body with pedicles (Figure 1). Mesh density was controlled by 5 parameters (see Appendix, [Supplemental Digital Content 1](#)), whose values were chosen to generate an accurate mesh with a limited computing time (about 10 minutes) resulting in FEMs with 4300 elements. Failure load varied by less than 5% when the number of elements was raised from 4300 to 34,000.

The geometry of the vertebral body mesh was compared with the 3D reconstruction of the vertebra by evaluating the distances from the external nodes of the mesh to the vertebral external surface. ²⁸

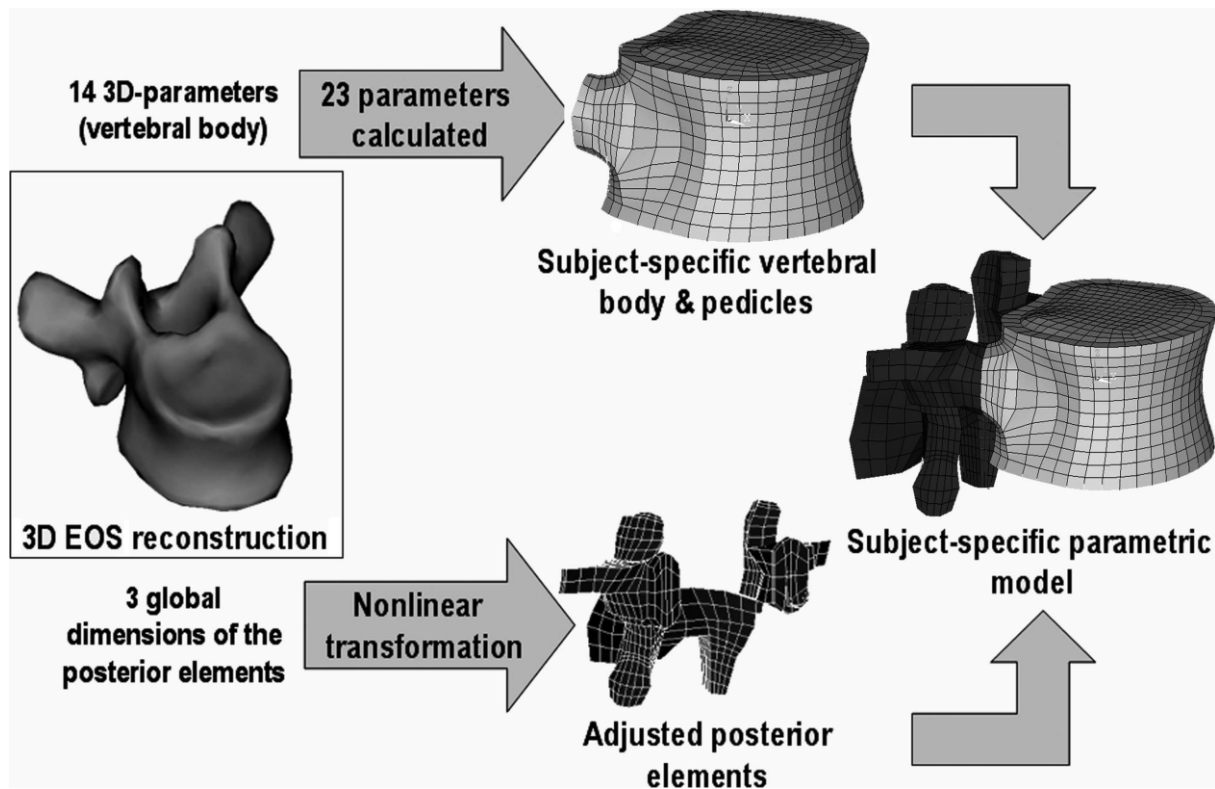


Figure 1. Subject-specific finite element modelling. The subject-specific vertebral body and the pedicles are generated using 23 parameters deduced from 14 measures on the EOS 3-dimensional reconstruction. The posterior elements, whose dimensions are adjusted, are then fixed to the pedicles.

Subject-Specific Mechanical Properties

Two homogeneous and isotropic materials with a linear elastic behavior were considered (Figure 2). Up to now, clinical imaging devices cannot provide *in vivo* accurate evaluation of the vertebral cortical thickness. Hence, a thick layer of a homogeneous material representing a mixing of cancellous and cortical bone, called “cortico-cancellous bone,” was designed around the central part of the vertebral body that represented the cancellous bone. The mechanical properties of the cancellous bone were assigned using a previously established aBMD–modulus relationship²⁰ (“subject-specific FEM”). To assess the contribution of these subject-specific mechanical properties for strength prediction, a model with average Young’s modulus was also designed for each vertebra (“average FEM” with $E_{\text{cancellous bone}} = 187 \text{ MPa}$ ²⁰). The Poisson ratio (ν) was set to 0.3. The cortico-cancellous bone attributes were taken from previous experiments²⁹: 22 samples made of cancellous and cortical bone were tested in compression, and the homogenized Young’s modulus of the material was computed by a finite element analysis with an inverse method.²⁹ To be in the same conditions as in this previous study, the thickness of the external cortico-cancellous layer of the vertebral model was equal to the thickness of the samples (3 mm,²⁹) and the Young’s modulus of the cortico-cancellous bone was the average of the homogenized bone stiffness computed for the 22 samples (374 MPa²⁹). ν was set to 0.3.

Failure Load Estimate

Loading Scenario

Experimental data for validation. The experimental protocol was described elsewhere.²³ The vertebral end plates were embedded in polymethacrylate cement layers. The vertebrae were compressed up to failure (displacement rate: 1 mm/min). They were submitted to an eccentric compressive load to generate compression and anterior bending. Rotation of the upper loading plate was allowed by means of a ball joint located in the anterior part of the vertebral body. At each time, the 3D position of the point of load application and the 3D orientation of the load were known relative to the vertebral local frame using an optoelectronic device (accuracy 0.6°). Vertical loads and displacements were assessed to validate the FEM. The error of the load measurement was 0.4% (8 N on average).

Boundary conditions of the finite element model. Cement layers were modeled (Young’s modulus $E_{\text{cement layer}} = 2500 \text{ MPa}$, $\nu = 0.3$; Figure 3). All the degrees of freedom were constrained on the polymethacrylate inferior face. The load was applied on a node whose location matched the specific 3D origin of the load during the experiment. Its 3D coordinates relative to the vertebra were computed from the magnitude of vertical load and the matrix of rotation that quantifies the 3D position of the vertebra relative to the testing machine. The load was transmitted to the superior face of the cement layer through high stiff beams (Young’s modulus $E_{\text{beam}} = 120,000 \text{ MPa}$, $\nu = 0.3$; Figure 3).

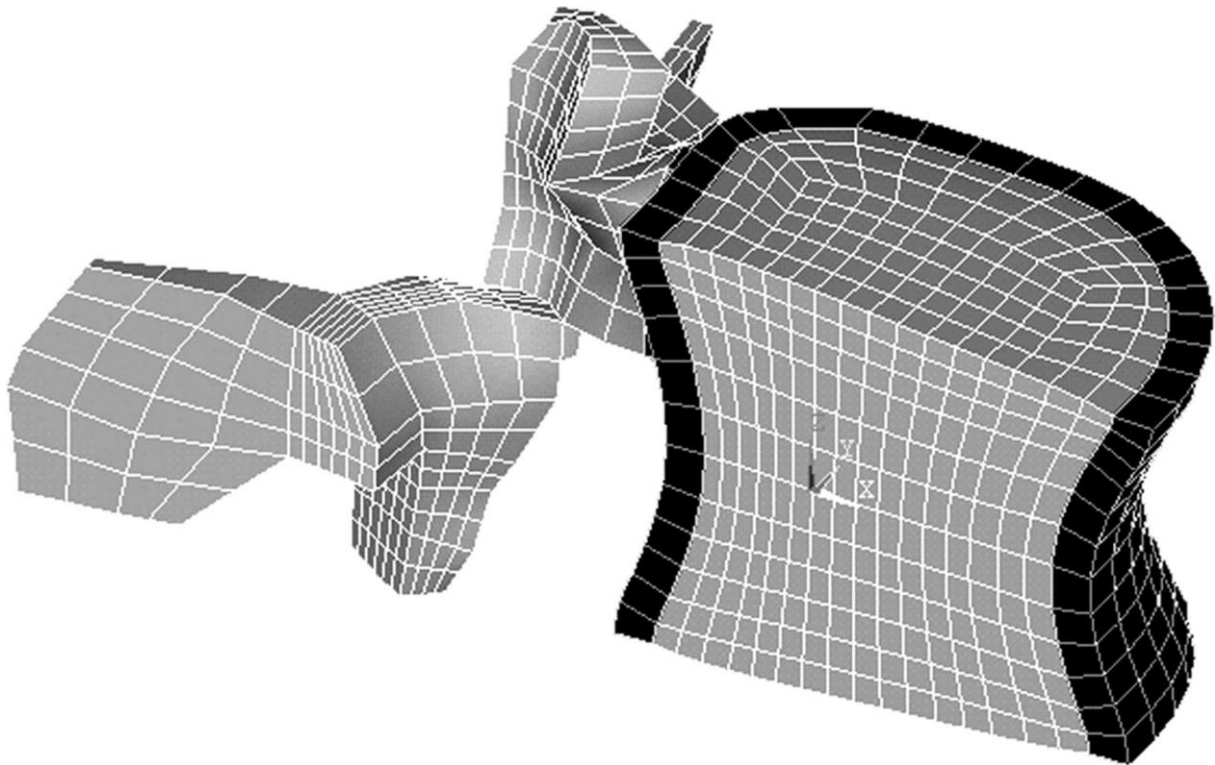


Figure 2. Sagittal cut of the vertebra. The vertebral body is composed of 2 homogeneous media: the cancellous bone (gray) surrounded by a cortico-cancellous shell (black).

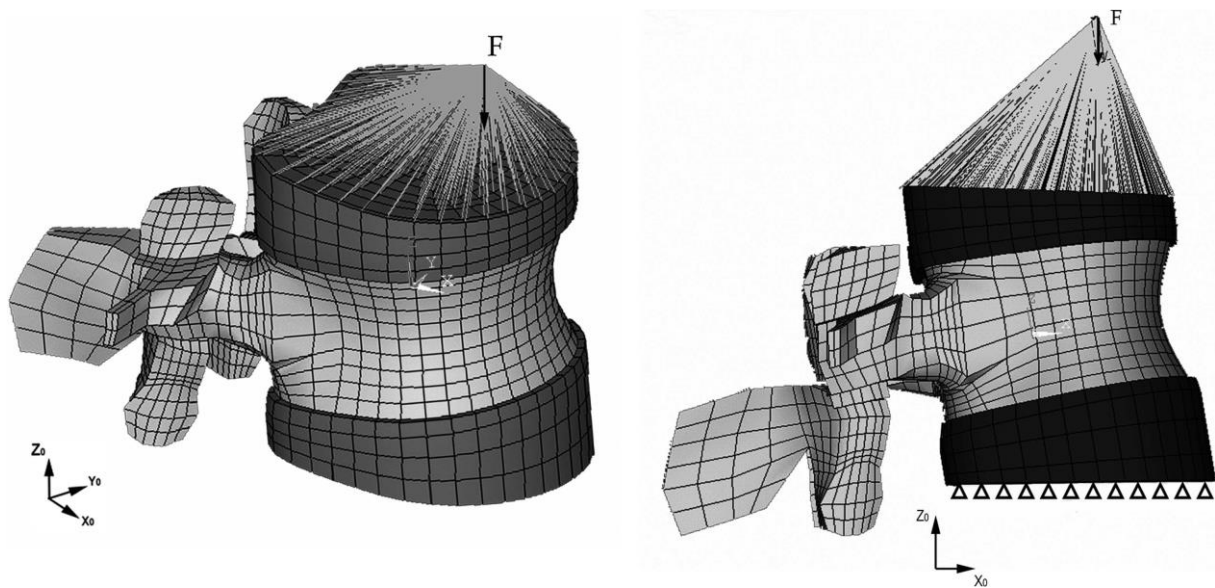


Figure 3. The boundary conditions match the experimental setup. PMMA layers (in dark gray) are modeled around the upper and lower vertebral end plates. Nodes of the inferior face of PMMA are locked. The load is applied at node “F,” whose coordinates correspond to the origin of the experimental load. The 3D coordinates of the load (vertical in the global frame $[X_0, Y_0, \text{ and } Z_0]$) relative to the vertebra (local frame $[X, Y, \text{ and } Z]$) are computed from the 3D orientation of the vertebra during the experiment and the magnitude of the load. 3D indicates 3 dimensional; PMMA, polymethacrylate.

Failure Load Estimate

Failure criterion. The virtual vertebra was set to fail when a significant volume of cortico-cancellous bone elements reached a maximum principal strain higher than their failure strain. The limit of the compressive elastic strain $|\epsilon_{3 \text{ max}}|$ was set to 1.5%, which corresponds to the maximum principal strain at failure for 22 cortico-cancellous samples.²⁹ The threshold volume of failed elements was chosen equal to 1 cm³ (median for the 14 vertebrae). The prediction of failure load depends on this volume. To quantify this effect, the failure load was computed for different values of volume from 0.4 cm³ to 1.6 cm³.

Statistical Analyses

Statistical analyses were performed using Matlab statistics toolbox (Matlab 7.5.0 [R2007b], The MathWorks Inc, Natick, MA). The relative error of prediction was quantified:

$$\text{Relative error} = \frac{|F_{FEM} - F_{exp}|}{F_{exp}} \quad (1)$$

where F_{FEM} is the computed failure load and F_{exp} is the experimental one.

Moreover, correlations between aBMD and experimental failure loads and between computed failure loads and experimental failure loads were quantified. Robust linear regressions using the bisquare weights robust method were made: it minimizes a weighted sum of squares, where the weight given to each data point depends on how far the point is from the fitted line. ³⁰ The adjusted coefficient of determination (r^2 adjusted), the P value, and the root mean square error of the estimate (RMSE) were expressed. $P = 0.05$ was the cut off for significance in all statistical analyses.

RESULTS

Accuracy of the Subject-Specific Mesh

The distance between the nodes of the subject-specific mesh (vertebral body with pedicles) and the external surface of the 3D reconstruction of the vertebra was, on average, equal to 1.0 ± 0.2 mm (95% of the point-to-surface distances were, on average, lower than 2.6 mm).

Influence of the Failure Criterion on Strength Prediction

Variation of the computed failure load linearly changes with the volume defining the failure criterion (Figure 4). Variations of the volume of failed elements up to 60% led to a variation of the computed failure load of 12% at most (approximately 250 N). The computed load changed by only 0.23% (approximately 4.5 N) when the volume varied 1.5% (variation of volume corresponding to 1 element). A volume of 1 cm^3 was kept for all the remaining simulations.

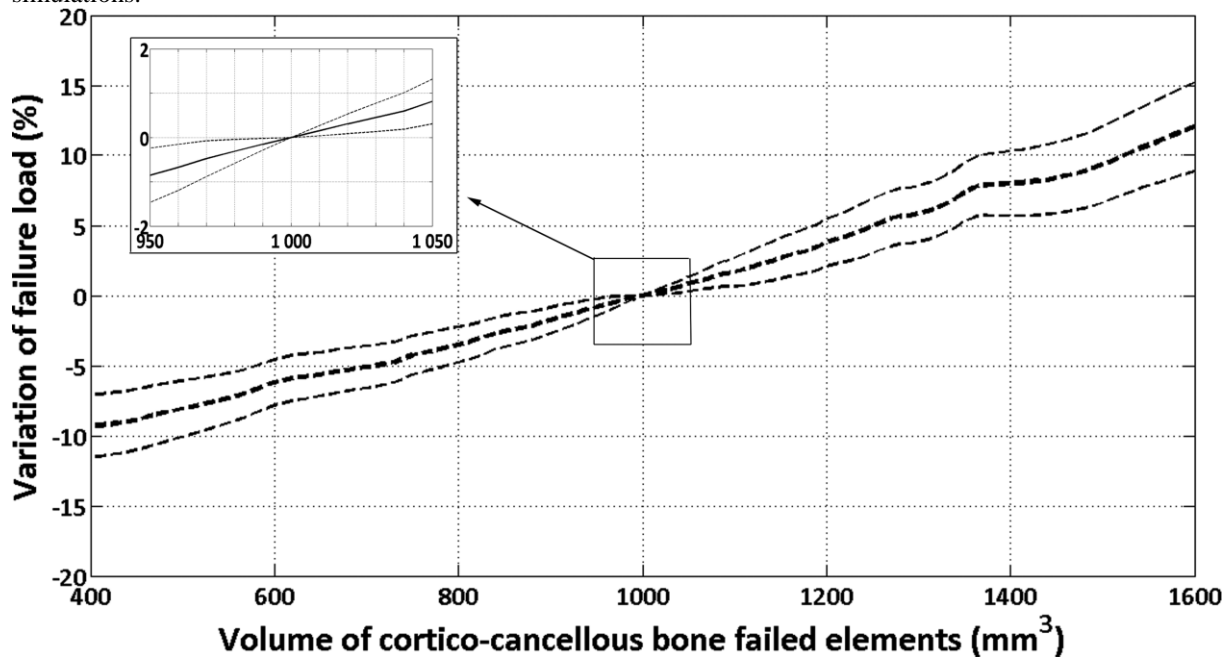


Figure 4. Influence of the volume of cortico-cancellous bone failed elements on the computed failure load. The variation of the failure load is computed for different threshold volumes of failed elements in the cortico-cancellous bone layer. The reference for the loads is the failure load computed with a volume of $1 \text{ cm}^3 = 1000 \text{ mm}^3$

Failure Load Estimate

The mean aBMD of the vertebrae was equal to $0.711 \pm 0.148 \text{ g/cm}^2$ ($0.527\text{--}1.024 \text{ g/cm}^2$). BMDs were not significantly correlated with *in vitro* vertebral failure loads (r^2 adjusted = 0.46, $P = 0.08$, RMSE = 646 N). The relative error of the failure load estimate (equation 1) decreased on average by 2.5-fold, when the subject-specific mechanical properties were implemented in the FEMs (16% vs. 43%, Figure 5 and Table 1). However, for 1 of the 14 vertebrae, the relative error was higher with the subject-specific FEM than with the average FEM.

Failure loads computed by average FEMs were not significantly correlated with experimental failure loads (r^2 adjusted = 0.01, $P = 0.71$). On the contrary, the correlation was significant with failure load computed by subject-specific models (r^2 adjusted = 0.79, $P = 5.10 \cdot 10^{-5}$, RMSE = 367 N; Figure 6). Two outliers (vertebra number 3 and 6) were identified by the robust fitting method. The model was able to separate vertebrae with either low or high

strength (failure load respectively lower or higher than 2500 N). Maximum compressive principal strains were located near the vertical projection of the node where the load is applied and preferentially in the cortico-cancellous shell.

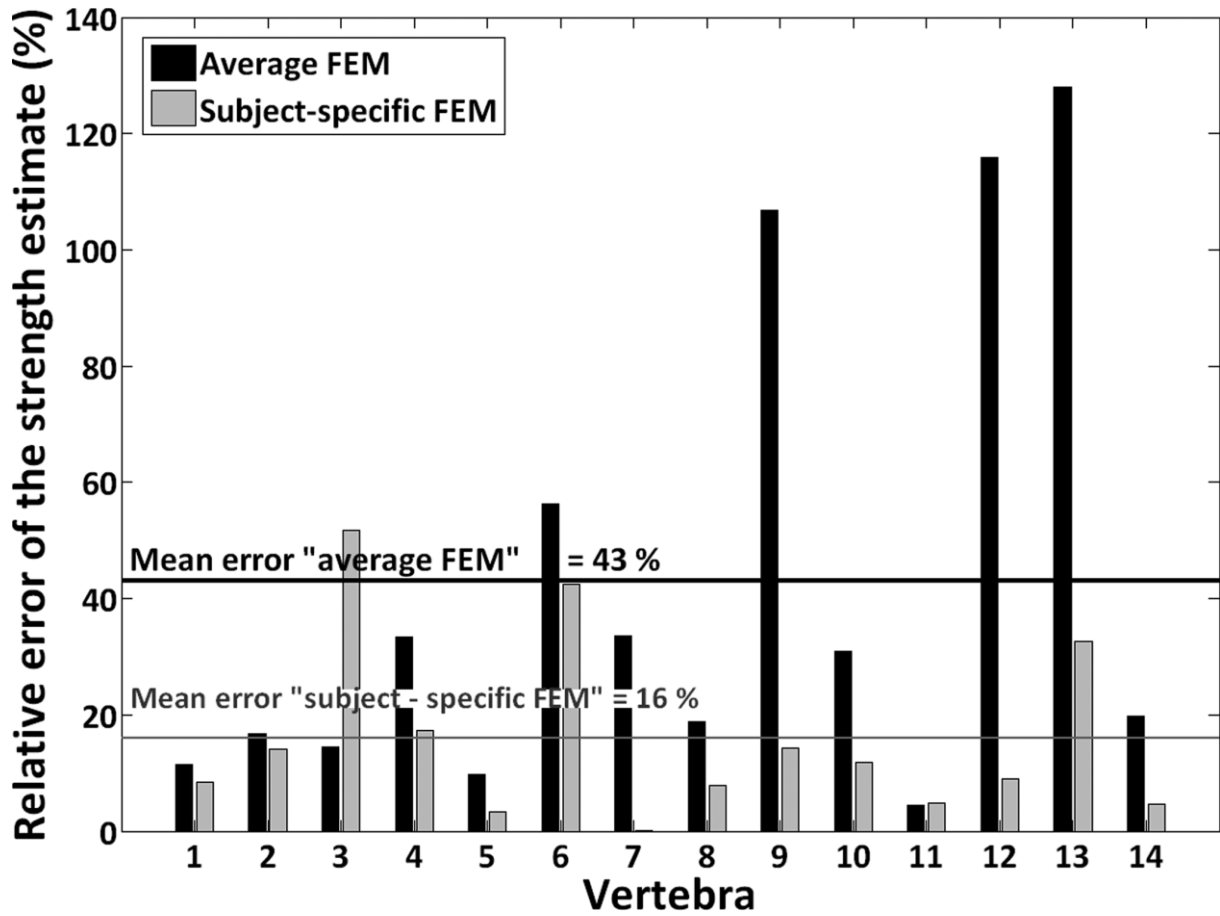


Figure 5. Influence of the subject-specific mechanical properties: relative error of prediction using “average FEMs” (with subject-specific geometry but averaged Young’s moduli) and “subject-specific FEMs” (with subject-specific geometry and Young’s modulus of cancellous bone). FEM indicates finite element model.

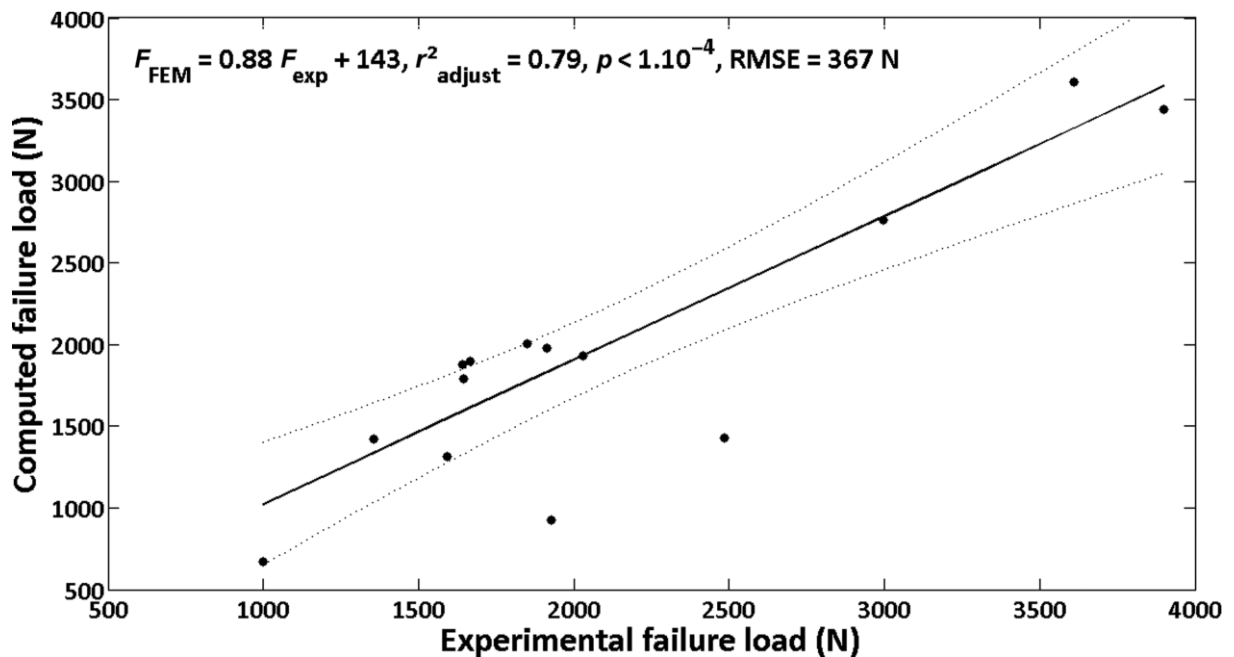


Figure 6. Correlation between experimental failure loads and computed failure load using “subject-specific finite element models.” Data points and robust linear fit (with 95% confidence bounds).

Table 1. Experimental Failure load (From Sapin et al.23) and computed failure loads for each vertebra.

Vertebra				Failure load (N)			Relative error of prediction (%)	
No.	Age	Sex	Level	Experimental	Average FEM	Subject-Specific FEM	Average FEM	Subject-Specific FEM
1	92	F	L1	1848	1635	2003	12	8
2	92	F	L2	1665	1945	1899	17	14
3	86	F	T11	1927	2205	929	14	52
4	86	F	L2	1593	2125	1316	33	17
5	65	M	T11	1914	2100	1976	10	3
6	65	M	T12	2484	1085	1428	56	43
7	65	M	L1	3611	2395	3608	34	0
8	65	M	L2	2997	2435	2762	19	8
9	92	F	T11	1642	3395	1876	107	14
10	92	F	L1	3900	2690	3438	31	12
11	92	F	L2	2031	1940	1932	5	5
12	103	F	T11	1645	3550	1794	116	9
13	103	F	T12	1000	2280	674	128	33
14	103	F	L1	1357	1090	1421	20	5

FEM indicates finite element model.

DISCUSSION

This study aims to create and evaluate subject-specific FEMs on the basis of a low-dose imaging modality, to predict the strength of thoracic and lumbar vertebrae. The vertebrae were submitted to an eccentric compression force leading to compression and anterior bending. This loading was chosen because anterior bending (attributable to pure moment or eccentric compression force) is responsible for wedge vertebral fractures.

Accuracy of the Subject-Specific Mesh

A smooth parametric mesh was preferred to a voxel-based approach, resulting in less numeric artefacts.^{31–34} The method used to obtain the mesh enables a fast modeling of a thoracic or lumbar vertebra. Its external surface matched with the 3D reconstruction of the vertebra. The posterior arch was modelled by a generic mesh with adjusted global dimensions. The geometry of the vertebral body and the pedicles was subject specific and close to the actual one (the average point-to-surface distance was equal to 1 mm, and 95% of distances were smaller than 2.6 mm).

Failure Load Estimate

Areal BMD only explains 46% of the failure load, which is consistent with results in the literature.^{2,3} However, the correlation was not significant ($P = 0.08$) in this study, contrary to previous works. This is probably because of the small number of spines considered. The correlation between failure loads computed with average FEMs and experimental failure loads was not significant. But, by implementing the subject-specific Young's modulus of cancellous bone in the model, the relative error between computed and experimental failure loads decreased 2.5-fold, and the failure load estimate was significant. It underlines the validity of the relationships predicting the Young's modulus of the cancellous bone from EOS BMD measurements.²⁰ Nevertheless, the subject-specific model was less predictive than the average model for 1 vertebra (vertebra 3). This vertebra had several big osteophytes, which are known to bias the BMD assessment. Consequently, the Young's modulus of the cancellous bone, deduced from the BMD, could be altered. Subject-specific FEMs predicted 79% of the vertebral failure load (significant correlation) with a 95% confidence interval equal to ± 734 N (35% of the average failure load). The power of this result is limited by the small number of vertebrae with high strength, even if it is counterbalanced by the use of robust statistical analyses. Robust regressions were chosen because least squares predictions are dragged toward the outliers and the variance of the estimates is artificially inflated, which results in masking outliers and biased estimations. This method identified 2 outliers, among which is the previously discussed vertebra number 3. Only a few spines with relatively advanced ages were included in the study. Thus, direct comparison of the statistical results (determination coefficient and P value) with those previously listed for QCT-based models is limited by the number of vertebrae. However, the prediction of vertebral strength ($r^2 = 0.79$) is close to the one with QCT-based FEM in axial

compression ($r^2 = 0.80-0.94$).⁷⁻¹⁰ Considering the eccentric loading in this study, the results could be compared to the prediction of QCT-based models in anterior bending.^{11, 12} Dall'Ara and colleagues'¹¹ study predicted 79% of the strength under eccentric compression, but they removed the vertebral end plates so that the loading conditions could not be compared with the present experiments. Buckley et al.¹² considered complete vertebral bodies. Direct comparison of the determination coefficients is not suited in this case because the number of vertebrae is different (13 vs. 30) as well as the loading mode (eccentric force vs. bending moment). Nevertheless, it is interesting to observe that the present scatter is obviously overlaid with data sets from Buckley and colleagues'¹² study (Figure 7). It shows that the level of prediction of the subject-specific FEMs on the basis of low-dose imaging is in the same range as one of the QCT-based models validated in anterior bending. As expected, the highest principal strains were concentrated at the anterior part of the vertebral body, at the maximum of curvature and near the vertical projection of the origin of the load. High strains were preferentially located in the cortico cancellous shell, which is stiffer. It suggests that the cortico cancellous shell significantly contributes to the vertebral strength in anterior compression as was previously indicated in the literature.¹⁰ Unfortunately, it was not possible to compare the computed strain fields with radiographic data because there was no line of fracture on the radiographs after the mechanical tests. Another limit of the study is that the level of prediction of the FEM is linked to the failure criterion. The use of a strain-based criterion was preferred to a criteria based on stresses because ultimate strain of human bone can be considered stable compared with ultimate stress for a given anatomical site,^{35, 36} and invariant to density.^{35, 37} The limit of strain was directly deduced from experimental data. Furthermore, the failure criterion was expressed in volume to be independent of the element size, but the volume of failed elements depends on the vertebrae studied. However, this influence was moderate because a variation of 60% of the volume induced a variation of 12% of the computed failure load. Finally, the vertebrae were made of isotropic and homogeneous media because the 3D variability of the mechanical properties was not computed from the biplanar EOS radiographs. The development of methods to assess tissue heterogeneity in the vertebral body from the distribution of the intensities on the EOS radiographs should improve the prediction of the failure load. In conclusion, subject-specific FEMs based on low-dose x-ray imaging are able to predict *in vitro* vertebral failure load. The relative error between computed and experimental failure loads decreased 2.5-fold by implementing the subject-specific Young's modulus of cancellous bone in the model. Considering the potential of improvements regarding the material properties (heterogeneity and anisotropy), the study yields promising results for further *in vivo* predictions of spinal strength.

Key Points

- FEMs based on EOS low-dose imaging are able to predict strength of vertebrae submitted to an eccentric compression leading to both compression and anterior bending ($r_2 = 0.79$, $P = 5.10^{-5}$, RMSE = 367 N).
- The prediction error is divided by 2.5 when subject specific mechanical properties, derived from a real BMD, are implemented in the FEM.
- Once adapted and validated *in vivo*, the method could improve the prediction of vertebral fracture risk.

Acknowledgments

The authors thank Stephanie Duverger and Nicolas Gémin for their participation in the design of the parametric finite element model. Supplemental digital content is available for this article.

References

1. National Institutes of Health . Osteoporosis prevention, diagnosis, and therapy . *NIH Consens Statement* 2000 ; 17 : 1 – 45 .
2. Bürklein D , Lochmüller EM , Kuhn V , et al. Correlation of thoracic and lumbar vertebral failure loads with in situ vs. ex situ dual energy X-ray absorptiometry . *J Biomech* 2001 ; 34 : 579 – 87 .
3. Ebbesen EN , Thomsen JS , Beck-Nielsen H , et al. Lumbar vertebral body compressive strength evaluated by dual-energy X-ray absorptiometry, quantitative computed tomography, and ashing . *Bone* 1999 ; 25 : 713 – 24 .
4. Lochmüller EM , Bürklein D , Kuhn V , et al. Mechanical strength of the thoracolumbar spine in the elderly: prediction from in situ dualenergy X-ray absorptiometry, quantitative computed tomography (QCT), upper and lower limb peripheral QCT, and quantitative ultrasound . *Bone* 2002 ; 31 : 77 – 84 .
5. Lochmüller EM , Eckstein F , Kaiser D , et al. Prediction of vertebral failure loads from spinal and femoral dual-energy X-ray absorptiometry, and calcaneal ultrasound: an in situ analysis with intact soft tissues . *Bone* 1998 ; 23 : 417 – 24 .
6. Cummings SR , Melton LJ . Epidemiology and outcomes of osteoporotic fractures . *Lancet* 2002 ; 359 : 1761 – 7 .
7. Buckley JM , Loo K , Motherway J . Comparison of quantitative computed tomography-based measures in predicting vertebral compressive strength . *Bone* 2007 ; 40 : 767 – 74 .
8. Crawford RP , Cann CE , Keaveny TM . Finite element models predict in vitro vertebral body compressive strength better than quantitative computed tomography . *Bone* 2003 ; 33 : 744 – 50 .
9. Crawford RP , Rosenberg WS , Keaveny TM . Quantitative computed tomography-based finite element models of the human lumbar vertebral body: effect of element size on stiffness, damage, and fracture strength predictions . *J Biomech Eng* 2003 ; 125 : 434 – 8 .
10. Chevalier Y , Pahr D , Zysset PK . The role of cortical shell and trabecular fabric in finite element analysis of the human vertebral body . *J Biomech Eng* 2009 ; 131 : 111003 .

11. Dall'Ara E, Schmidt R, Pahr D, et al. A nonlinear finite element model validation study based on a novel experimental technique for inducing anterior wedge-shape fractures in human vertebral bodies in vitro . *J Biomech* 2010 ; 43 : 2374 – 80 .
12. Buckley JM , Cheng L , Loo K , et al. Quantitative computed tomography- based predictions of vertebral strength in anterior bending . *Spine* 2007 ; 32 : 1019 – 27 .
13. McDonnell P , Harrison N , McHugh PE . Investigation of the failure behaviour of vertebral trabecular architectures under uni-axial compression and wedge action loading conditions . *Med Eng Phys* 2010 ; 32 : 569 – 76 .
14. Lunt M , O'Neill TW , Felsenberg D , et al. European Prospective Osteoporosis Study Group . Characteristics of a prevalent vertebral deformity predict subsequent vertebral fracture: results from the European Prospective Osteoporosis Study (EPOS) . *Bone* 2003 ; 33 : 505 – 13 .
15. Gangnet N , Pomero V , Dumas R , et al. Variability of the spine and pelvis location with respect to the gravity line: a three-dimensional stereoradiographic study using a force platform . *Surg Radiol Anat* 2003 ; 25 : 424 – 33 .
16. Dubouset J , Charpak G , Dorion I , et al. A new 2D and 3D imaging approach to musculoskeletal physiology and pathology with low-dose radiation and the standing position: the EOS system . *Bull Acad Natl Med* 2005 ; 189 : 287 – 97 .
17. Humbert L , De Guise JA , Aubert B , et al. 3D reconstruction of the spine from biplanar X-rays using parametric models based on transversal and longitudinal inferences . *Med Eng Phys* 2009 ; 31 : 681 – 7 .
18. Pomero V , Mitton D , Laporte S , et al. Fast accurate stereoradiographic 3D-reconstruction of the spine using a combined geometric and statistic model . *Clin Biomech* 2004 ; 19 : 240 – 7 .
19. Sapin E , Briot K , Kolta S , et al. Bone mineral density assessment using the EOS low-dose X-ray device: a feasibility study . *Proc Inst Mech Eng H* 2008 ; 222 : 1263 – 71 .
20. Sapin-De Broses E , Briot K , Kolta S , et al. Subject-specific mechanical properties of cancellous bone assessment using a low-dose X-ray device . *IRBM* 2010 ; 31 : 148 – 53 .
21. Lafage V , Schwab F , Skalli W , et al. Standing balance and sagittal plane spinal deformity: analysis of spinopelvic and gravity line parameters . *Spine* 2008 ; 33 : 1572 – 8 .
22. Steffen J-S , Obeid I , Aurouer N , et al. 3D postural balance with regard to gravity line: an evaluation in the transversal plane on 93 patients and 23 asymptomatic volunteers . *Eur Spine J* 2009 ; 19 : 760 – 7 .
23. Sapin E , Chan F , Ayoub G , et al. Anterior bending on whole vertebrae using controlled boundary conditions for model validation . *J Musculoskelet Res* 2009 ; 12 : 71 – 6 .
24. Duchemin L , Mitton D , Jolivet E , et al. An anatomical subject-specific FE-model for hip fracture load prediction . *Comput Methods Biomech Biomed Engin* 2008 ; 11 : 105 – 11 .
25. Lavaste F , Skalli W , Robin S , et al. Three-dimensional geometrical and mechanical modelling of the lumbar spine . *J Biomech* 1992 ; 25 : 1153 – 64 .
26. Laporte S , Mitton D , Ismael IB , et al. Quantitative morphometric study of thoracic spine. A preliminary parameters statistical analysis. *Eur J Orthop Surg Traumatol* 2011 ; 49 : 1355 – 61 .
27. Travert C , Jolivet E , Sapin-de Broses E , et al. Sensitivity of patient specific vertebral finite element model from low dose imaging to material properties and loading conditions . *Med Biol Eng Comput* 2011;49:1355–61 .
28. Mitulescu A , Semaan I , De Guise J , et al. Validation of the non stereo corresponding points stereoradiographic 3D reconstruction technique . *Med Biol Eng Comput* 2001 ; 39 : 152 – 8 .
29. El Masri F , Sapin E , Rhissassi K , et al. Apparent Young's modulus of vertebral cortico-cancellous bone specimens . *Comput Methods Biomech Biomed Engin* [published online ahead of print July 13,2011.] DOI: 10.1080/10255842.2011.565751.
30. Fox J . *Applied Regression Analysis, Linear Models, and Related Methods* . Thousand Oaks, CA : SAGE ; 1947 .
31. Boyd SK . Image-based finite element analysis . In: Sensen CW , Hallgrímsson B . *Advanced Imaging in Biology and Medicine* . Berlin, Germany : Springer ; 2009 : 301 – 18 .
32. Chevalier Y , Pahr D , Zysset PK . Comparison of voxel-based and smooth finite element models to predict damage accumulation in vertebral bodies . Montréal, Québec, Canada : Presented at: 30th Annual Meeting of the American Society of Bone and Mineral Research ; September 12–16, 2008 .
33. Niebur GL , Yuen JC , Hsia AC , et al. Convergence behavior of highresolution finite element models of trabecular bone . *J Biomech Eng* 1999 ; 121 : 629 – 35 .
34. Pahr D , Zysset PK . A comparison of enhanced continuum FE with micro FE models of human vertebral bodies . *J Biomech* 2009 ; 42 : 455 – 62 .
35. Kopperdahl DL , Keaveny TM . Yield strain behavior of trabecular bone . *J Biomech* 1998 ; 31 : 601 – 8 .
36. Morgan EF , Keaveny TM . Dependence of yield strain of human trabecular bone on anatomic site . *J Biomech* 2001 ; 34 : 569 – 77 .
37. Cowin SC , He QC . Tensile and compressive stress yield criteria for cancellous bone . *J Biomech* 2005 ; 38 : 141 – 4 .